AJNR

The Role of Preload and Leakage Correction in Gadolinium-Based Cerebral Blood Volume Estimation Determined by Comparison with MION as a Criterion Standard

J. L. Boxerman, D.E. Prah, E.S. Paulson, J.T. Machan, D. Bedekar and K.M. Schmainda

AJNR Am J Neuroradiol 2012, 33 (6) 1081-1087
doi: https://doi.org/10.3174/ajnr.A2934
http://www.ajnr.org/content/33/6/1081

ORIGINAL RESEARCH

The Role of Preload and Leakage Correction in Gadolinium-Based Cerebral Blood Volume Estimation Determined by Comparison with MION as a Criterion Standard

J.L. Boxerman
D.E. Prah
E.S. Paulson
J.T. Machan
D. Bedekar
K.M. Schmainda

BACKGROUND AND PURPOSE: Contrast extravasation in DSC-MRI potentiates inaccurate and imprecise estimates of glioma rCBV. We tested assertions that preload and postprocessing algorithms minimize this error by comparing Gd-rCBV using permutations of these 2 techniques with criterion standard rCBV using MION, an intravascular agent.

MATERIALS AND METHODS: We imaged 7 Fisher rats with 9L gliosarcomas, by using 3T gradient-echo DSC-MRI with MION (2.0 mg Fe/kg) and staged injection of Gd-diethylene triamine pentaacetic acid: a 0.1-mmol/kg bolus provided no preload (P−) data and served as preload (P+) for a subsequent 0.2-mmol/kg bolus. We computed MION-rCBV (steady-state $\Delta R2^*$, tumor versus normal brain) and Gd-rCBV $\Delta R2^*$ [t] integration) without (C−) and with (C+) postprocessing correction, thereby testing 4 correction permutations: P−C−, P−C+, P+C−, and P+C+. We tested whether each permutation reduced bias and variance of the Gd/MION rCBV differences by using generalized estimating equations and Fmax statistics ($P < .05$ significant).

RESULTS: Gd-rCBV progressively better approximated MION-rCBV with increasing leakage correction. There was no statistically significant bias for the mean percentage deviation of Gd-rCBV from MION-rCBV for any correction permutation, but there was significantly reduced variance by using P+C− (22-fold), P−C+ (32-fold), and P+C+ (267-fold) compared with P−C−. P+C+ provided significant additional variance reduction compared with P+C− (12-fold) and P−C+ (8-fold). Linear regression of Gd-rCBV versus MION-rCBV revealed P+C+ to have the closest slope and intercept compared with the ideal, substantially better than P+C−.

CONCLUSIONS: Preload and postprocessing correction significantly reduced the variance of Gd-rCBV estimates, and bias reduction approached significance. Postprocessing correction provide significant benefit beyond preload alone.

ABBREVIATIONS: C− = without leakage correction algorithm applied; C+ = with leakage correction algorithm applied; CI = confidence interval; DSC = dynamic susceptibility contrast; Gd = gadolinium; K2 = linear coefficient in the fitting algorithm used to correct for contrast agent extravasation in CBV estimates as defined in References 21 and 22; MION = monocrystalline iron oxide nanoparticle intravascular contrast agent; P− = without administration of preload contrast agent dose; P+ = with administration of preload contrast agent dose; rCBV = relative cerebral blood volume

When confined to the intravascular space, paramagnetic contrast agents (eg, Gd-diethylene triamine pentaacetic acid) produce T2*-weighted signal intensity loss in the extravascular space, and DSC-MRI rCBV maps are computed by integrating the transverse relaxivity changes ($\Delta R2^*$) that occur dynamically over a first-pass injection.[1,2] There has been extensive clinical application of rCBV mapping during the past decade to the imaging of gliomas, including grading[3-7] and prognosis[8-10] at initial diagnosis; targeting biopsy[11,12] and providing intraoperative guidance;[13] predicting low-grade to high-grade transformation;[14,15] and monitoring response to treatment,[16,17] including the distinction of tumor recurrence and posttreatment-related enhancement due to radiation necrosis[18] and pseudoprogression.[19,20]

In enhancing high-grade gliomas with substantial blood-brain barrier breakdown, typical Gd-based contrast agents extravasate, reducing T2* DSC-MRI signal intensity loss by signal intensity increase in regions where T1 effects are significant.[21,22] In such instances, rCBV will be underestimated and may even be "negative" in highly permeable lesions with rapid contrast extravasation where T1 effects overwhelm the intravascular T2* effects, severely blunting or even eliminating any perceived first-pass susceptibility bolus effect. Conversely, T2* effects due to susceptibility differences between extravasated contrast in the extracellular space and tumor cells

Received August 29, 2011; accepted after revision September 26.

From the Departments of Diagnostic Imaging (J.L.B.) and Orthopedics and Surgery (J.T.M.), Rhode Island Hospital and Alpert Medical School of Brown University, Providence, Rhode Island; and Departments of Radiation Oncology (D.E.P., E.S.P.), Biophysics (K.M.S.), and Radiology (D.B., K.M.S.), Medical College of Wisconsin, Milwaukee, Wisconsin.

Paper previously presented in part at: Annual Meeting of the American Society of Neuroradiology, June 7–14, 2007; Chicago, Illinois.

This work was supported by NIH/National Cancer Institute RO1 CA082500; Advancing a Healthier Wisconsin; and MCW Translational Brain Tumor Research Program.

Please address correspondence to Jerrold L. Boxerman, MD, PhD, Department of Diagnostic Imaging, Rhode Island Hospital, 593 Eddy St, Providence, RI 02903; e-mail: jboxerman@lifespan.org

http://dx.doi.org/10.3174/ajnr.A2934

Table 1: Techniques for reducing T1 leakage effects

Category	Technique	Examples
Image acquisition	Low flip angle, long TE, double-echo T2*-weighted	Knopp et al,[11] Cha et al[38] Vonken et al,[27] Uematsu et al[28]
Contrast agent	Use of loading doses[a]	Donahue et al,[3] Schmainda et al,[21] Simonsen et al[35]
	Intravascular agents (eg, ferumoxytol)	Gahramanov et al[20]
Postprocessing	Linear fit + leakage model[a]	Weisskoff et al,[31] Schmainda et al[21] Boxerman et al[22]
	γ-Variate fit	Law et al[4]
	Limited integration	Wong et al[30]
	Baseline subtraction	Wetzel et al[29]

[a] Designates the 2 techniques investigated in this article.

can increase $\Delta R2^*$.[23] Due to this complex interplay of T1- and T2-weighted effects, contrast agent leakage can lead to either underestimation or overestimation of rCBV in enhancing tumors unless specifically corrected for.[23-25] Because clinical decisions for the applications mentioned above increasingly rely on rCBV quantitation for analysis of temporal trends and absolute thresholds, it is paramount that the DSC technique be optimized to prevent or correct these inaccuracies and ensure that rCBV measurements are accurate and precise.

Whereas early studies neglected leakage-effect contamination,[26] more recent studies have acknowledged this pitfall, with most correction schemes focusing on the T1 effects. Generally speaking, T1 leakage-correction schemes can be broadly classified into 3 groups (Table 1): image acquisition (low flip angle, long TE gradient-echo;[11,16] double-echo T2*-weighted[27,28]), contrast agent selection (loading dose of contrast agent before DSC-MRI to minimize subsequent changes in T1;[3,21] intravascular agents such as ferumoxytol[20]), and postprocessing techniques (parametric modeling such as γ-variate fit;[1,4] baseline subtraction;[29] limited integration;[30] and mathematic leakage-correction models[21-23,25,31,32]).

A robust mathematic leakage-correction model was proposed by Weisskoff et al,[21,22,31] which uses linear fitting to determine the voxelwise deviation from nonleaky reference tissue and, by removing the leakage term, generates corrected rCBV values and first-order estimates of vascular permeability. This postprocessing technique is appealing because it does not require nonstandard imaging sequences or contrast agent injection schemes; however, though it theoretically improves rCBV estimation, there is only anecdotal evidence for its effectiveness. For instance, rCBV maps generated with a prebolus loading dose of contrast plus the correction scheme of Weisskoff et al significantly correlate with glioma tumor grade, whereas uncorrected maps do not.[22,24] To our knowledge, there has been no formal validation of the preload and postprocessing correction techniques against a criterion standard. The purpose of this study was to determine the degree to which Gd-based rCBV estimates, by using this increasingly common combination of leakage-correction techniques, match criterion standard rCBV measured with a purely intravascular contrast agent (MION; Massachusetts General Hospital Center for Molecular Imaging Research, Charlestown, Massachusetts). We hypothesized that correction schemes using both techniques would perform better than schemes using only 1 or none, as measured by smaller variance of Gd/MION rCBV ratios and reduced bias.

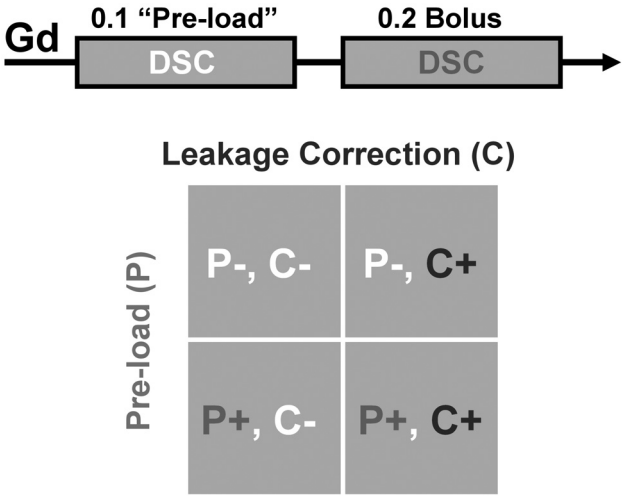

Fig 1. Summary of Gd-based DSC methodology: staged injection technique. Gradient-echo DSC-MRI (0.1-mmol/kg gadodiamide bolus) provides no preload (P−) rCBV data and serves as a preload (P+) for subsequent DSC-MRI (0.2 mmol/kg bolus). Gd-rCBV without (C−) and with (C+) application of postprocessing leakage correction are computed for both P− and P+ data, thereby testing P−C−, P−C+, P+C−, and P+C+ permutations of the 2 leakage-correction techniques.

Materials and Methods

Intracranial Xenograft Transplantation in Rats

Seven male Fisher rats (Charles River Laboratories, Wilmington, Massachusetts) were anesthetized and immobilized, and 10^5 9L gliosarcoma cells were injected through a 0.9-mm calvarial burr-hole (1 mm anterior and 2 mm lateral to the bregma) into the right frontal lobe 3 mm deep to the dura.[33] Care of rats followed the National Institutes of Health *Guide for the Care and Use of Laboratory Animals* (1996). The Institutional Animal Care and Use Committee at the Medical College of Wisconsin approved all protocols.

MR Imaging

Fourteen days following tumor cell inoculation, MRI was performed (3T Signa Excite; GE Healthcare, Milwaukee, Wisconsin; quadrature birdcage coil; FOV = 4 cm, 4 sections, 2-mm section thickness). DSC-MRI (gradient-echo EPI, TR = 1 second, TE = 34.5 ms, matrix = 64 × 64, 60 seconds before and 60 seconds after injection) was performed with both MION (2.0 mg Fe/kg bolus) and gadodiamide (Omniscan; GE Healthcare) in each rat, with randomly assigned order. For gadodiamide-based DSC-MRI, we used a staged injection technique (Fig 1). Dynamic imaging during an initial single-dose bolus (0.1 mmol/kg) provided no preload (P−) rCBV data and served as preload (P+) for subsequent DSC-MRI using a double-dose (0.2 mmol/kg) bolus. Single-dose (P−) and double-dose (P+) injections were separated by 10 minutes. Finally, T1-weighted spin-echo images (TE/TR = 12/450 ms, 256 × 256 matrix, NEX = 16) were acquired to delineate enhancing tumor.

rCBV Computation

Using custom AFNI-based[34] postprocessing software (Bloomington, Illinois), we converted signal intensity time curves to relaxivity time curves ($\Delta R2^*[t]$) for each voxel by using a standard technique. For initial (P−) and secondary (P+) injection data, we estimated Gd-

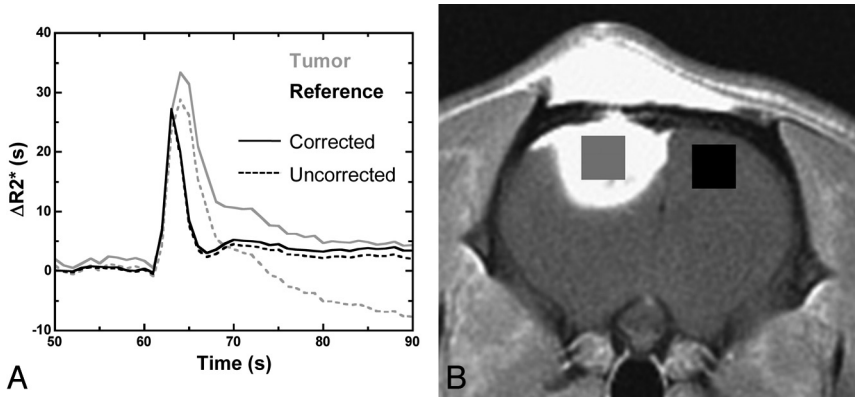

Fig 2. Gd-rCBV for initial (P−) and second (P+) injection data was computed by using voxelwise trapezoidal integration of $\Delta R2^*(t)$ without (C−) and with (C+) postprocessing leakage correction. *A*, Examples of P+C− and P+C+ curves in tumor and reference brain. *B*, The ratio of mean rCBV from tumor (gray) and contralateral brain (black) ROIs was computed for all injections, providing normalized rCBV values.

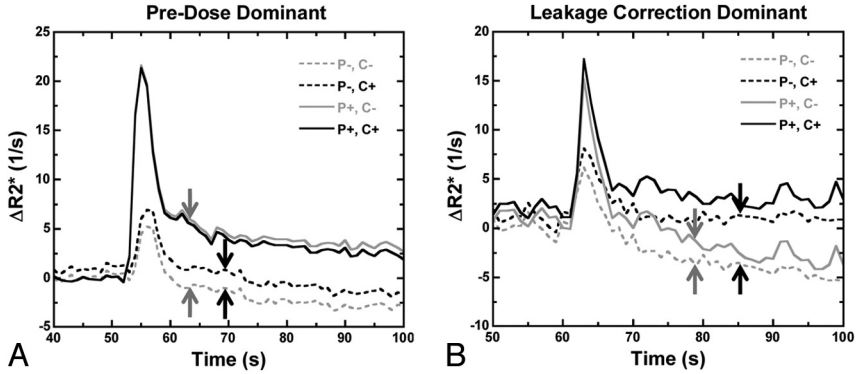

Fig 3. Comparison of preload-dominant and postprocessing-dominant corrective effects on relaxivity time curves for 2 different tumors. *A*, Preload alone (solid gray line) eliminates most of the T1 leakage contamination (*dashed gray line* with blunted peak relaxivity and negative $\Delta R2^*$ values; shift between *gray arrows*), whereas postprocessing correction does not (*dashed black line*; shift between *black arrows*). *B*, Postprocessing algorithm has more substantial corrective effect than preload in the tail portion of the curves (*dashed black* versus *dashed gray lines*; shift between *black* versus *gray arrows*), but the converse is true during the first pass (*solid* versus *dashed lines*), demonstrating synergy between the 2 correction schemes. Combining preload and postprocessing (*solid black lines*) yields the greatest peak $\Delta R2^*$ without negative relaxivity values.

rCBV without (C−) and with (C+) application of a leakage-correction algorithm based on the linear fit of uncorrected $\Delta R2^*(t)$ to constant functions derived from nonenhancing brain parenchyma,[21,22] thereby testing all 4 permutations of the 2 leakage-correction techniques (P−C−, P−C+, P+C−, and P+C+; see Fig 2*A* for examples of P+C− and P+C+ curves in tumor and reference brain). We generated rCBV maps for each permutation by using numeric trapezoidal integration of $\Delta R2^*(t)$ over all time points on a voxelwise basis. ROIs of enhancing tumor and normal-appearing reference brain were determined from the postcontrast T1-weighted spin-echo images and coregistered to the rCBV maps for each rat (Fig 2*B*). Mean rCBV values from the tumor ROI and the reference ROI were extracted, and their ratio was computed, providing a normalized rCBV value for each leakage-correction permutation in all rats.

We used MION, an intravascular agent with high T2 relaxivity, as a criterion standard for tumor rCBV, because this agent does not extravasate. Tumor MION-rCBV was estimated by computing the ratio of the steady-state $\Delta R2^*$ relaxivity value in tumor to that in reference brain by using the same ROIs.[35]

Data Analysis and Statistical Methods

For each rat, Gd-rCBV estimates from each leakage-correction permutation were normalized to the criterion standard MION-rCBV as a percentage difference (Gd-rCBV − MION-rCBV / MION-rCBV). Using a generalized estimating equation for normally distributed data, we modeled the percentage differences as a function of preload (P+ versus P−), leakage correction (C+ versus C−), and their interaction and tested whether each correction permutation reduced bias and variance of Gd/MION-rCBV ratios by using F_{max} statistics (http://www.biology.ed.ac.uk/research/groups/jdeacon/statistics/table8.htm) (Holm-adjusted $P < .05$ was considered significant when comparing correction schemes with each other; unadjusted P values used when comparing correction schemes with ideal or null values). The variances for each correction permutation and covariances between them were modeled by using sandwich estimators and assuming independent variances. The relationships between Gd-rCBV and MION-rCBV for each correction permutation were determined by using another generalized estimating equation that compared slopes and intercepts with the ideal (zero intercept and unity slope) and, in the case of slopes, also with a null of zero, indicating no relationship.

Results

Figure 3 compares the relative effects of preload and the postprocessing algorithm on individual relaxivity time curves. In some tumors, the postprocessing algorithm without preload had minimal corrective effect, whereas inclusion of preload had substantial restorative effects (preload dominant, Fig 3*A*). In other tumors, the opposite was true, with more substantial corrective effect from the postprocessing algorithm (postprocessing dominant; Fig 3*B*). These illustrations suggest a com-

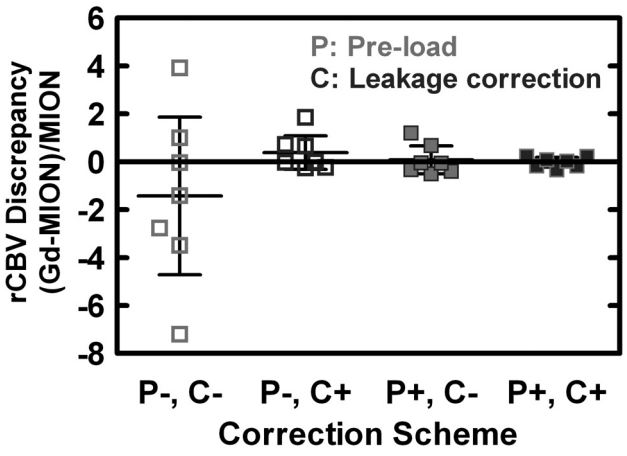

Fig 4. Comparison of rCBV discrepancies ([Gd − MION] / MION) for each correction scheme permutation (mean and 95% CI). Although there is no statistically significant intrascheme or interscheme bias, mean discrepancy is closest to zero for P+C+ (−1.8%), followed by P+C− (+7.6%), P−C+ (+38.3%), and P−C− (−142.8%). The variance of rCBV discrepancies differed substantially between correction schemes, with P+C− (22-fold), P−C+ (32-fold), and P+C+ (267-fold) all statistically significantly lower compared with P−C−. The use of both correction techniques (P+C+) further significantly reduced the variance compared with that for each individually (12-fold versus P+C−, 8-fold versus P−C+).

plementary role of the 2 leakage-correction schemes. Combining preload and postprocessing algorithms (solid black lines) yields the most robust relaxivity time curves, with the greatest peak $\Delta R2^*$ and the absence of negative relaxivity values.

Figure 4 compares the rCBV discrepancies ([Gd − MION] /MION) for each of the 4 correction-scheme permutations (mean, 95% CI). Without preload or leakage-correction algorithms, Gd-rCBV estimates are very discordant, and 3 of the 7 Gd-rCBV values were negative before correction. Although there was no statistically significant bias within or between correction schemes, the mean discrepancy was closest to the ideal of zero for P+C+, followed by P+C−, P−C+, and P−C− (Table 2). There were substantial differences in the variance of discrepancies for the different correction schemes; compared with the variance for P−C−, the variance of discrepancies was statistically significantly lower for P+C− (22-fold, adjusted $P = .003$), P−C+ (32-fold, adjusted $P = .01$), and P+C+ (267-fold, adjusted $P < .0001$). Although there was no significant difference between the variances for P+C− and P−C+ (1.5-fold, adjusted $P = .67$), the use of both correction techniques (P+C+) further significantly reduced the variance compared with that for each individually (12-fold versus P+C−, adjusted $P = .01$; 8-fold versus P−C+, adjusted $P = .02$).

Because the interscheme differences in variance were so striking, we examined the specific relationship between Gd-rCBVs and MION-rCBVs for each correction permutation (Table 2). The intercepts for P−C−, P+C−, and P−C+ each differed significantly from the ideal of zero, whereas the intercept for P+C+ did not. Although the slopes for P−C−, P+C−, P−C+, and P+C+ differed significantly from the ideal of 1, P−C+ ($P = .03$) and P+C+ ($P = .009$) produced statistically significant evidence of a greater-than-chance relationship between Gd-rCBV and MION-rCBV, whereas P−C− and P+C− did not. In Fig 5, Gd-rCBV with preload and with (P+C+) and without (P+C−) postprocessing correction is plotted against MION-rCBV. The linear fit for rCBV data with postprocessing correction is much closer to identity than the linear fit without, arguing that the use of both correction schemes outperforms the use of only 1.

Discussion

Our results offer strong evidence that the combination of preload and postprocessing correction schemes significantly reduces the variance of Gd-rCBV measures relative to criterion standard MION-rCBV compared with either technique alone and no correction. The results also suggest that both techniques may reduce the tendency toward bias observed without correction. The practical implication is that the combined correction scheme improves the accuracy and precision of Gd-rCBV measurements, which is important for clinical applications such as the evaluation of posttreatment gliomas that rely on rCBV quantitation for analysis of temporal trends and absolute thresholds.

Extravasated contrast shortens the extravascular-extracellular compartment T1, counteracting the transient first-pass susceptibility contrast-induced signal intensity drop used to estimate tumor hemodynamics. Preload administration minimizes T1 leakage contamination by saturating the baseline extravascular-extracellular compartment T1-weighted signal intensity, thereby diminishing T1-induced signal intensity increases during subsequent DSC-MRI. It may also reduce the gradient of contrast efflux. The importance of the preload cannot be overemphasized[3] and may be the difference between an indiscernible and robust signal intensity drop in very leaky tumors. In some cases without preload, no signal intensity drop is detectable in the signal intensity time curve; in such cases, it may be impossible to "resurrect" legitimate DSC-MRI data by using the postprocessing algorithm. Although the postprocessing algorithm may provide sufficient leakage correction in cases with robust signal intensity drop in the absence of preload, our results suggest a synergistic effect between these 2 techniques, and we advocate their use in tandem.

Preload dose and other factors such as "incubation" time between preload and secondary bolus may impact the adequacy of preload leakage correction.[36] Hu et al[36] found that a 0.1-mmol/kg preload dose and a 6-minute incubation time helped optimize discrimination of posttreatment-related enhancement and tumor progression compared with uncorrected rCBV measurement, and our use of a 0.1-mmol/kg preload and 10-minute incubation time would certainly be in line with that recommendation. We kept the preload dose and incubation time constant to reduce preload-related variance in Gd-rCBV.

The postprocessing algorithm used herein generates both corrected rCBV maps and first-order estimates of vascular permeability.[22] In addition to signal intensity contamination by competing T1 effects, contrast extravasation may also diminish $\Delta R2^*$ by decreasing the magnetic susceptibility gradient between the intra- and extravascular spaces ($\Delta\chi$). However, susceptibility differences created between extravascular contrast and tumor cells may increase $\Delta R2^*$, providing cell attenuation sensitivity on DSC-MRI, which may help distinguish common enhancing malignant lesions.[37] For example, the postbolus plateau of the relaxivity time curves in Fig 3 does not completely return to baseline, even after leakage correc-

Table 2: Summary of discrepancy between Gd-rCBV and MION-rCBV for each correction scheme permutation

Scheme	rCBV Discrepancy		Intercept		Slope	
	Mean (%)	95% CI (%)	Mean	95% CI	Mean	95% CI
P−C−	−142.8	−471.5, +186.0	+1.4	+1.1, +1.6	−0.01	−0.04, +0.02
P−C+	+38.3	−32.0, +108.6	+1.3	+0.8, +1.8	+0.16	+0.02, +0.31
P+C−	+7.6	−50.1, +65.9	+1.0	+0.5, +1.5	+0.02	−0.29, +0.33
P+C+	−1.8	−22.0, +18.3	+0.6	−0.2, +1.4	+0.58	+0.17, +1.00

Note:—rCBV discrepancy indicates (Gd-rCBV − MION-rCBV) / MION-rCBV (ideal equals zero); intercept and slope, the linear fit of MION-rCBV versus Gd-rCBV (ideal equals zero intercept with unity slope).

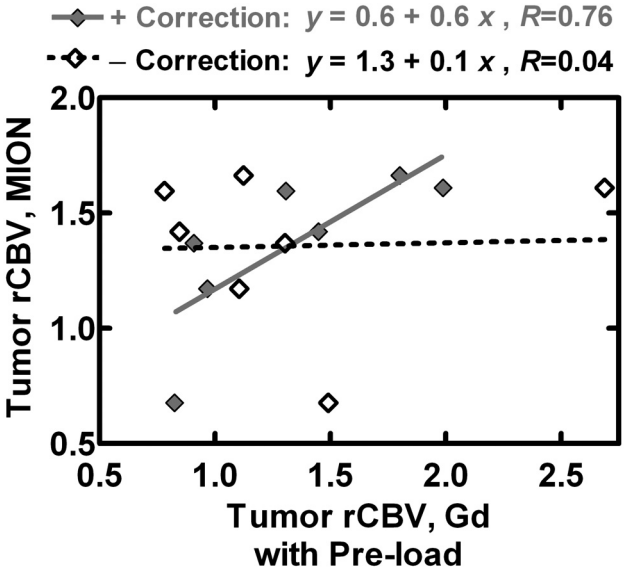

Fig 5. Gd-rCBV with preload and with (P+C+) and without (P+C−) leakage correction is plotted against MION-rCBV. The linear fit for P+C+ data is much closer to the ideal line of identity than the linear fit for P+C−, arguing that the use of both correction schemes outperforms the use of only preload.

tion, representing extravasation-related residual T2* effects. The complex interplay between T1- and T2*-weighted effects on DSC-MRI signal intensity is an active area of investigation.[23-25]

Other postprocessing correction techniques exist. γ-variate fitting eliminates tail deviation of $\Delta R2^*(t)$ due to extravasation[4,11] but would not correct first-pass amplitude reduction (Fig 3*B*), is nonlinear, is often unstable, and has SNR deficiencies.[2,38] Early bolus extravasation may be substantial in high-grade tumors with high vascular permeability, and ignoring first-pass amplitude reduction could yield large rCBV inaccuracies. Considering only peak $\Delta R2^*$ or only integrating from bolus onset to peak $\Delta R2^*$ ("limited integration method"[30]) does not account for first-pass $\Delta R2^*$ suppression or late bolus $\Delta R2^*$ effects. The "baseline subtraction method"[29] assumes that the $\Delta R2^*(t)$ tail matches the initial baseline, with homogeneous linear contamination throughout the first pass. The postprocessing model used herein approximately corrects the entire relaxivity time curve by using a stable linear fit, permitting numeric integration during the entire first pass, with associated advantages in accuracy and rCBV SNR.[2]

There are alternatives to preload with postprocessing correction for minimizing rCBV error. Double-echo T2*-weighted DSC-MRI uses signal intensities at 2 different TEs and an exponential model to compute $\Delta R2^*(t)$ without T1 contamination.[27,28] This may still have T2* contamination but, if corrected for, significantly correlates with tumor grade, performing on a par, in this sense, with the preload/postprocessing correction scheme; these 2 methods appear to provide the most robust rCBV estimation in the setting of contrast agent extravasation.[24] We think that addressing T1 leakage correction remains important because preload/postprocessing correction schemes are becoming commonplace and well cited. Furthermore, residual T2* contamination effects can still confound rCBV estimates, and to the extent that the postprocessing correction herein also addresses T2* contamination (included in the K2 term), the preload/postprocessing correction technique provides some degree of comprehensive leakage correction.

Similar to previously investigated iron oxide contrast agents,[39,40] high-molecular-weight intravascular iron-containing agents with large susceptibility effects (eg, ferumoxytol) would eliminate the need for any leakage correction entirely.[41,42] However, they may introduce practical issues with regard to T1-weighted postcontrast imaging, given that extravasation accounts for most enhancement associated with conventional Gd-based agents. For example, in an intrapatient comparison of gadoteridol and ferumoxytol in intracranial tumors, ferumoxytol rCBV values were significantly larger ($P = .0016$) than gadoteridol rCBV values[43]; this finding implies a reduction of T1 leakage contamination.

We found that several Gd-rCBV estimates were negative for the P−C− group, likely due to a predominance of negative $\Delta R2^*$ secondary to avid contrast enhancement; numeric integration through the tail in such instances can accumulate large negative $\Delta R2^*$. This begs the question of how the temporal limits of $\Delta R2^*$ integration are selected. We collected images for 60 seconds during and after bolus injection, typically yielding 40–50 images following the first pass. It could be argued that an abbreviated integration strategy as previously discussed could minimize sensitivity to T1 leakage effects and reduce the variance of rCBV estimates. However, our methodology mimics that in previous publications documenting significant correlation of rCBV with tumor grade.[22,24] Furthermore, the postprocessing correction technique extends the useful observation time in the dynamic phase of the contrast bolus, potentially increasing the contrast-to-noise ratio of the computed rCBV maps.[2] The trend toward negative bias for the P−C− case illustrates the fact that T1 contamination, by affecting the first pass and/or tail of the relaxivity time curve, tends to artificially lower rCBV estimates.

The second of our staged bolus injections (P+ cases) was a double-dose injection, compared with a single-dose injection for P− cases, and this would certainly affect the relative SNR of P+ versus P− rCBV measures and consequently the relative

group variances. This injection strategy mimics commonly published techniques, though because of nephrogenic systemic fibrosis risk and higher molar T1 relaxivity of newer contrast agents (eg, gadobenate dimeglumine, MultiHance; Bracco Imaging, Milan, Italy; gadobutrol, Gadovist; Bayer Schering Pharma, Berlin-Wedding, Germany), we reduce the preload at our institution to one-fourth dose followed by a single-dose dynamic bolus. This experiment could be repeated to confirm the suspected relevance of our conclusions at this different dosing strategy. In any event, we demonstrated significant variance reduction for P+C+ compared with P+C−, and P−C+ compared with P−C−, both at the same dosing protocols, suggesting the added benefit of postprocessing correction in both preload scenarios.

Because neovascularity in high-grade gliomas is characterized by disorganized large-scale microvessels,[44] we used gradient-echo EPI because it has $\Delta R2^*$ sensitivity to microvessels of all sizes, contrary to spin-echo with peak $\Delta R2^*$ sensitivity to capillary-sized microvessels.[45] Furthermore, gradient echo–based rCBV is known to be a statistically significant predictor of tumor grade,[22] and gradient-echo EPI is probably the most commonly used DSC technique. Nonetheless, we expect that the results of this study should pertain to spin-echo–based rCBV measures as well.

Limitations to our study include a relatively small sample size and the single-versus-double-dose contrast boluses used for P− and P+ cases, respectively. Although multiple investigators have used the postprocessing algorithm tested herein, the limitations of this reference-correction method have been identified, including sensitivity to MTT, whereby elevated tumor MTT may cause rCBV underestimation due to incorrect estimation of K2.[25] This may affect comparative rCBV estimates between tumor and reference tissue or between high- and low-grade gliomas typically having relatively lower and higher MTT, respectively. Bjornerud et al[25] proposed a novel postprocessing correction algorithm that is insensitive to MTT variations, and the use of more sophisticated postprocessing correction schemes may further improve the residual variance in the P+C+ scheme and the regression of Gd-rCBV estimates versus MION-rCBV criterion standard.

Conclusions

The rat gliosarcoma model with MION provides a viable model for testing T1 leakage-correction schemes against criterion standard rCBV measures. Conventional single-dose rCBV estimates without leakage correction correlate very poorly with true rCBV and should not be trusted in high-grade tumors. Both preload and the postprocessing correction algorithms independently reduce the variance of Gd-rCBV estimates, but there is an additional benefit when used in tandem. It is an ongoing work in our laboratories to better understand and reduce T2* and latent susceptibility components of rCBV error; the MION rat model may be helpful for achieving this goal.

Acknowledgments

We thank Stuart B. Boxerman for his insightful comments regarding the statistical analysis of the data.

Disclosures: Devyani Bedakar—No disclosures. Kathleen Schmainda—*UNRELATED: Patents (planned, pending, or issued)*: Several patents have been filed on MRI technology developments;* *Royalties*: Royalties received due to Medical College of Wisconsin licensing copyright to Imaging Biometrics LLC; *Other*: Imaging Biometrics LLC, *Comments*: ownership interest. *Money paid to the institution.

References

1. Rosen BR, Belliveau JW, Vevea JM, et al. **Perfusion imaging with NMR contrast agents.** *Magn Reson Med* 1990;14:249–65
2. Boxerman JL, Rosen BR, Weisskoff RM. **Signal-to-noise analysis of cerebral blood volume maps from dynamic NMR imaging studies.** *J Magn Reson Imaging* 1997;7:528–37
3. Donahue KM, Krouwer HG, Rand SD, et al. **Utility of simultaneously acquired gradient-echo and spin-echo cerebral blood volume and morphology maps in brain tumor patients.** *Magn Reson Med* 2000;43:845–53
4. Law M, Yang S, Babb JS, et al. **Comparison of cerebral blood volume and vascular permeability from dynamic susceptibility contrast-enhanced perfusion MR imaging with glioma grade.** *AJNR Am J Neuroradiol* 2004;25:746–55
5. Spampinato MV, Smith JK, Kwock L, et al. **Cerebral blood volume measurements and proton MR spectroscopy in grading of oligodendroglial tumors.** *AJR Am J Roentgenol* 2007;188:204–12
6. Emblem KE, Scheie D, Due-Tonnessen P, et al. **Histogram analysis of MR imaging-derived cerebral blood volume maps: combined glioma grading and identification of low-grade oligodendroglial subtypes.** *AJNR Am J Neuroradiol* 2008;29:1664–70
7. Morita N, Wang S, Chawla S, et al. **Dynamic susceptibility contrast perfusion weighted imaging in grading of nonenhancing astrocytomas.** *J Magn Reson Imaging* 2010;32:803–08
8. Law M, Oh S, Johnson G, et al. **Perfusion magnetic resonance imaging predicts patient outcome as an adjunct to histopathology: a second reference standard in the surgical and nonsurgical treatment of low-grade gliomas.** *Neurosurgery* 2006;58:1099–107
9. Hirai T, Murakami R, Nakamura H, et al. **Prognostic value of perfusion MR imaging of high-grade astrocytomas: long-term follow-up study.** *AJNR Am J Neuroradiol* 2008;29:1505–10
10. Law M, Young RJ, Babb JS, et al. **Gliomas: predicting time to progression or survival with cerebral blood volume measurements at dynamic susceptibility-weighted contrast-enhanced perfusion MR imaging.** *Radiology* 2008;247:490–98
11. Knopp EA, Cha S, Johnson G, et al. **Glial neoplasms: dynamic contrast-enhanced T2*-weighted MR imaging.** *Radiology* 1999;211:791–98
12. Maia AC Jr, Malheiros SM, da Rocha AJ, et al. **Stereotactic biopsy guidance in adults with supratentorial nonenhancing gliomas: role of perfusion-weighted magnetic resonance imaging.** *J Neurosurg* 2004;101:970–76
13. Ulmer S, Helle M, Jansen O, et al. **Intraoperative dynamic susceptibility contrast weighted magnetic resonance imaging (iDSC-MRI): technical considerations and feasibility.** *Neuroimage* 2009;45:38–43
14. Law M, Oh S, Babb JS, et al. **Low-grade gliomas: dynamic susceptibility-weighted contrast-enhanced perfusion MR imaging–prediction of patient clinical response.** *Radiology* 2006;238:658–67
15. Danchaivijitr N, Waldman AD, Tozer DJ, et al. **Low-grade gliomas: do changes in rCBV measurements at longitudinal perfusion-weighted MR imaging predict malignant transformation?** *Radiology* 2008;247:170–78
16. Cha S, Knopp EA, Johnson G, et al. **Dynamic contrast-enhanced T2-weighted MR imaging of recurrent malignant gliomas treated with thalidomide and carboplatin.** *AJNR Am J Neuroradiol* 2000;21:881–90
17. Essock-Burns E, Lupo JM, Cha S, et al. **Assessment of perfusion MRI-derived parameters in evaluating and predicting response to antiangiogenic therapy in patients with newly diagnosed glioblastoma.** *J Neurooncol* 2011;13:119–31
18. Barajas RF Jr, Chang JS, Segal MR, et al. **Differentiation of recurrent glioblastoma multiforme from radiation necrosis after external beam radiation therapy with dynamic susceptibility-weighted contrast-enhanced perfusion MR imaging.** *Radiology* 2009;253:486–96
19. Hu LS, Baxter LC, Smith KA, et al. **Relative cerebral blood volume values to differentiate high-grade glioma recurrence from post-treatment radiation effect: direct correlation between image-guided tissue histopathology and localized dynamic susceptibility-weighted contrast-enhanced perfusion MR imaging measurements.** *AJNR Am J Neuroradiol* 2009;30:552–58
20. Gahramanov S, Raslan AM, Muldoon LL, et al. **Potential for differentiation of pseudoprogression from true tumor progression with dynamic susceptibility-weighted contrast-enhanced magnetic resonance imaging using ferumoxytol vs. gadoteridol: a pilot study.** *Int J Radiat Oncol Biol Phys* 2011;79:514–23
21. Schmainda KM, Rand SD, Joseph AM, et al. **Characterization of a first-pass gradient-echo spin-echo method to predict brain tumor grade and angiogenesis.** *AJNR Am J Neuroradiol* 2004;25:1524–32
22. Boxerman JL, Schmainda KM, Weisskoff RM. **Relative cerebral blood volume maps corrected for contrast agent extravasation significantly correlate with glioma tumor grade, whereas uncorrected maps do not.** *AJNR Am J Neuroradiol* 2006;27:859–67

23. Quarles CC, Gochberg DF, Gore JC, et al. **A theoretical framework to model DSC-MRI data acquired in the presence of contrast agent extravasation.** *Phys Med Biol* 2009;54:5749–66
24. Paulson ES, Schmainda KM. **Comparison of dynamic susceptibility-weighted contrast-enhanced MR methods: recommendations for measuring relative cerebral blood volume in brain tumors.** *Radiology* 2008;249:601–13
25. Bjornerud A, Sorensen AG, Mouridsen K, et al. **T(1)- and T(2)(*)-dominant extravasation correction in DSC-MRI. Part I. Theoretical considerations and implications for assessment of tumor hemodynamic properties.** *J Cereb Blood Flow Metab* 2011;31:2041–53. Epub 2011 Apr 20
26. Aronen HJ, Pardo FS, Kennedy DN, et al. **High microvascular blood volume is associated with high glucose uptake and tumor angiogenesis in human gliomas.** *Clin Cancer Res* 2000;6:2189–200
27. Vonken EP, van Osch MJ, Bakker CJ, et al. **Simultaneous quantitative cerebral perfusion and Gd-DTPA extravasation measurement with dual-echo dynamic susceptibility contrast MRI.** *Magn Reson Med* 2000;43:820–27
28. Uematsu H, Maeda M, Sadato N, et al. **Blood volume of gliomas determined by double-echo dynamic perfusion-weighted MR imaging: a preliminary study.** *AJNR Am J Neuroradiol* 2001;22:1915–19
29. Wetzel SG, Cha S, Johnson G, et al. **Relative cerebral blood volume measurements in intracranial mass lesions: interobserver and intraobserver reproducibility study.** *Radiology* 2002;224:797–803
30. Wong JC, Provenzale JM, Petrella JR. **Perfusion MR imaging of brain neoplasms.** *AJR Am J Roentgenol* 2000;174:1147–57
31. Weisskoff RM, Boxerman JL, Sorensen AG, et al. **Simultaneous blood volume and permeability mapping using a single Gd-based contrast injection.** In: *Proceedings of the Second Meeting of the Society of Magnetic Resonance,* San Francisco, California. August 6–12, 1994:279
32. Johnson G, Wetzel SG, Cha S, et al. **Measuring blood volume and vascular transfer constant from dynamic, T(2)*-weighted contrast-enhanced MRI.** *Magn Reson Med* 2004;51:961–68
33. Quarles CC, Ward BD, Schmainda KM. **Improving the reliability of obtaining tumor hemodynamic parameters in the presence of contrast agent extravasation.** *Magn Reson Med* 2005;53:1307–16
34. Cox RW. **AFNI: software for analysis and visualization of functional magnetic resonance neuroimages.** *Comput Biomed Res* 1996;29:162–73
35. Simonsen CZ, Ostergaard L, Vestergaard-Poulsen P, et al. **CBF and CBV measurements by USPIO bolus tracking: reproducibility and comparison with Gd-based values.** *J Magn Reson Imaging* 1999;9:342–47
36. Hu LS, Baxter LC, Pinnaduwage DS, et al. **Optimized preload leakage-correction methods to improve the diagnostic accuracy of dynamic susceptibility-weighted contrast-enhanced perfusion MR imaging in posttreatment gliomas.** *AJNR Am J Neuroradiol* 2010;31:40–48
37. Mangla R, Kolar B, Zhu T, et al. **Percentage signal recovery derived from MR dynamic susceptibility contrast imaging is useful to differentiate common enhancing malignant lesions of the brain.** *AJNR Am J Neuroradiol* 2011;32:1004–10
38. Cha S, Knopp EA, Johnson G, et al. **Intracranial mass lesions: dynamic contrast-enhanced susceptibility-weighted echo-planar perfusion MR imaging.** *Radiology* 2002;223:11–29
39. Loubeyre P, De Jaegere T, Bosmans H, et al. **Comparison of iron oxide particles (AMI 227) with a gadolinium complex (Gd-DOTA) in dynamic susceptibility contrast MR imagings (FLASH and EPI) for both phantom and rat brain at 1.5 Tesla.** *J Magn Reson Imaging* 1999;9:447–53
40. Enochs WS, Harsh G, Hochberg F, et al. **Improved delineation of human brain tumors on MR images using a long-circulating, superparamagnetic iron oxide agent.** *J Magn Reson Imaging* 1999;9:228–32
41. Neuwelt EA, Varallyay CG, Manninger S, et al. **The potential of ferumoxytol nanoparticle magnetic resonance imaging, perfusion, and angiography in central nervous system malignancy: a pilot study.** *Neurosurgery* 2007;60:601–11
42. Varallyay CG, Muldoon LL, Gahramanov S, et al. **Dynamic MRI using iron oxide nanoparticles to assess early vascular effects of antiangiogenic versus corticosteroid treatment in a glioma model.** *J Cereb Blood Flow Metab* 2009;29:853–60
43. Dosa E, Guillaume DJ, Haluska M, et al. **Magnetic resonance imaging of intracranial tumors: intra-patient comparison of gadoteridol and ferumoxytol.** *J Neurooncol* 2011;13:251–60
44. Zama A, Tamura M, Inoue HK. **Three-dimensional observations on microvascular growth in rat glioma using a vascular casting method.** *J Cancer Res Clin Oncol* 1991;117:396–402
45. Boxerman JL, Hamberg LM, Rosen BR, et al. **MR contrast due to intravascular magnetic susceptibility perturbations.** *Magn Reson Med* 1995;34:555–66